文章编号: 1001 - 9014(2018)04 - 0393 - 06

DOI:10.11972/j.issn.1001 - 9014.2018.04.003

Radio-frequency modeling and parameter extraction of graphene on-chip spiral inductors

ZHANG Yi-Xin, ZHANG Ao, WANG Bo-Ran, GAO Jian-Jun*

(School of Information Science and Technology, East China Normal University, Shanghai 200062, China)

Abstract: An improved equivalent circuit model for graphene spiral inductors based on physical principles is presented in this letter. The model is a π-circuit with additional parallel *RC* network in the series branch. A parameter extraction approach for proposed model, which combines the analytical approach and empirical optimization procedure, is also investigated. Good agreement is obtained between the simulated and measured *S*-parameters up to 40 GHz.

Key words: equivalent circuit, parameter-extraction approach, graphene inductor

PACS: 85. 30. De

石墨烯片上螺旋电感的射频建模和参数提取

张译心, 张 傲, 王博冉, 高建军*

(华东师范大学 信息科学技术学院 电子工程系,上海 200062)

摘要:基于物理原理,对石墨烯螺旋电感提出了一种改进的等效电路模型,该模型在传统π模型的串联支路中增加了*RC*并联网络.并结合分析法和优化法,对此模型提出了一种参数提取方法.结果表明,在1~40 GHz频率范围内,测试所得*S*参数和模型仿真所得*S*参数能够高度地吻合.

关 键 词:等效电路;参数提取方法;石墨烯电感

中图分类号:TN386.6 **文献标识码**:A

Introduction

On-chip spiral inductor, with low cost and ease of process integration, has been widely applied in radio-frequency integrated circuits such as RF amplifiers, mixers, voltage-controlled oscillators, and impedance-matching circuits[1-2]. With the emergence of 5G communication system, conventional metal passives are facing challenges for their high loss caused by skin effect in high-frequency circuit. Graphene, with extraordinary electrical and thermal conductivity, is a promising material for high-frequency applications including low-loss interconnects and passives[3]. Theoretical works[4-5] have identified that graphene pose to be a very attractive candidate for high-quality inductor design due to its large momentum relaxation time, and planar nature which enable graphene be patterned using high-resolution lithography without the need of metal conducts in carbon nanotube bundle-based inductors. References 3 reported the design and fabrication of graphene on-chip inductors.

Accurate modeling and modeling parameters extraction techniques for on-chip inductors is extremely important for optimizing the device performance and understanding the device physical mechanisms[6]. Many researchers have reported the modeling of conventional metal inductors[2,6-10] and parameter extraction methods[11-12, 14]. Most of them are based on a π-like topology[2, 7], with other modified double-π model[10] and T-model[8-9]. However, the high-frequency behavior of graphene pose a new problem for the design of modeling. The physical model for graphene inductors proposed in Ref. 3, composed of many elements, suffers from the difficulties of parameter extraction. The frequency-dependent elements in the simplified model[3] are also difficult to implement in time-domain simulators such as SPICE[2].

Received date: 2018-1-17, **revised date**: 2018-04-22 **收稿日期**:2018-1-17, **修回日期**:2018-04-22

Foundation items:Supported by National Natural Science Foundation of China (61474044)

Biography:ZHANG Yi-Xin (1993-), female, master, Shanghai, China. Research area involves modeling of devices and circuits. E-mail: yxzhang_ecnu@163.com

* **Corresponding author**:E-mail: jjgao@ee.ecnu.edu.cn

To overcome these restrictions, an improved equivalent circuit model that utilize only frequency independent elements, along with the parameter extraction method, is proposed. This paper is organized as follows. Sect. 1 gives the proposed equivalent circuit model of graphene on-chip inductors, which compared with conventional model. In Sect. 2, the basic procedure for extracting the model parameters is presented. Sect. 3 discusses the extraction results. The conclusions are given in Sect. 4.

1 Model of inductors

1.1 Device structure

The schematic view of test-structure layout and the graphene on-chip inductor are shown in Fig. 1[15] and Fig. 2, respectively. To implement the inductor, the prepared multilayer graphene films are transferred onto SiO_2 (300 nm)/ Si (10 Ω · cm) substrate firstly. Subsequently, graphene films are patterned into ribbon coils and an isolation dielectric layer (Al_2O_3:50 nm) is grown over the graphene multi-turn inductors. In the final step, metal contacts and pads (Ni/Au: 20 nm/80 nm) are deposited and patterned, followed by an annealing process[3]. By using de-embedding technology, which process is described by Ref. 3 and Ref. 13, the parasitic effects of test structure can be eliminated and measured *S*-parameters of the single graphene spiral inductor are actually needed for the following modeling process.

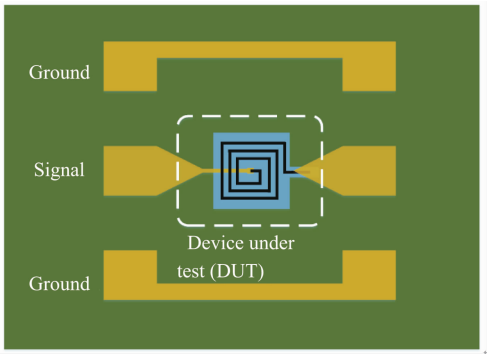

Fig. 1 Schematic view of test structure
图 1 测试结构示意图

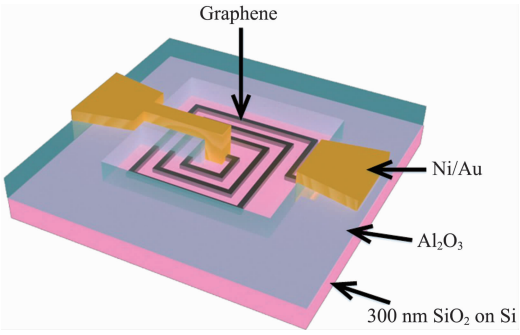

Fig. 2 Schematic of graphene inductor
图 2 石墨烯电感结构示意图

1.2 Conventional equivalent circuit model

A traditional single π-model is used to characterize the performance of a spiral inductor on silicon[7], as shown in Fig. 3. The model is composed of three segments: the series branch, which consists of L_{s0}, R_{s0}, L_{s1} and R_{s1}, and two shunt branches, modeled by C_{ox}, C_{si} and R_{si}. L_{s0} and R_{s0} represent the inductance and resistance of the spiral and underpass, respectively. The skin effect is modeled by the parallel inductance and resistance L_{s1} and R_{s1}. C_{ox} represents the oxide capacitance whereas R_{si} and C_{si} represent the silicon substrate resistance and capacitance, respectively.

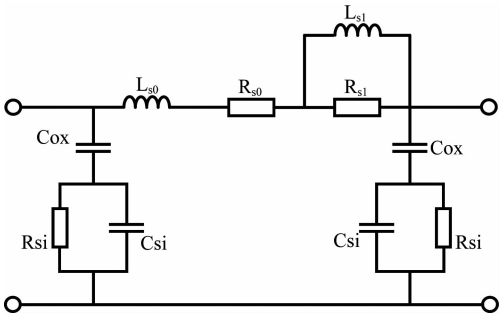

Fig. 3 Conventional π-model of metal inductors
图 3 传统的 π 型电感等效电路模型

The equivalent series resistance $R_s(f)$ and series inductance $L_s(f)$ were extracted from Y_{12}, the transmission admittance between two ports, which is transformed from de-embedded *S*-parameters, as follows:

$$R_s(f) + j\omega L_s(f) = -\frac{1}{Y_{12}} \quad . \quad (1)$$

And the quality factor was evaluated by

$$Q = -\frac{\mathrm{Im}(Y_{11})}{\mathrm{Re}(Y_{11})} \quad , \quad (2)$$

where Y_{11} is the input admittance of the circuit.

The skin effect has been taken into account in the conventional equivalent circuit model. The parallel L_{s1} and R_{s1} are added to model both the drop of series inductance L_s and the increase of series resistance R_s. In Ref. 13, useful approximate formulas were derived for predicting increases in equivalent series resistance with frequency, as follows:

$$R_s = R_{DC}\left[1 + \frac{1}{10}\left(\frac{\omega}{\omega_{crit}}\right)^2\right] \quad , \quad (3)$$

where ω_{crit} means the frequency at which the current crowding begins to become significant:

$$\omega_{crit} = \frac{3.1}{\mu_0}\frac{P}{W^2}R_{sheet} \quad , \quad (4)$$

where P is the turn pitch, W is the trace width and R_{sheet} means the trace's sheet resistance.

However, the high-frequency behavior of the graphene inductor is contrary to conventional metal inductors, as shown in Fig. 4. R_s and L_s remain approximately constant before 20 GHz, but R_s shows continued declines in the frequency range of 20 ~ 40 GHz while L_s rises significantly in this range. Thus, a new equivalent circuit is needed to model these characteristics over the entire frequency range.

1.3 Improved equivalent circuit model

Considering the drop-down of series resistance and

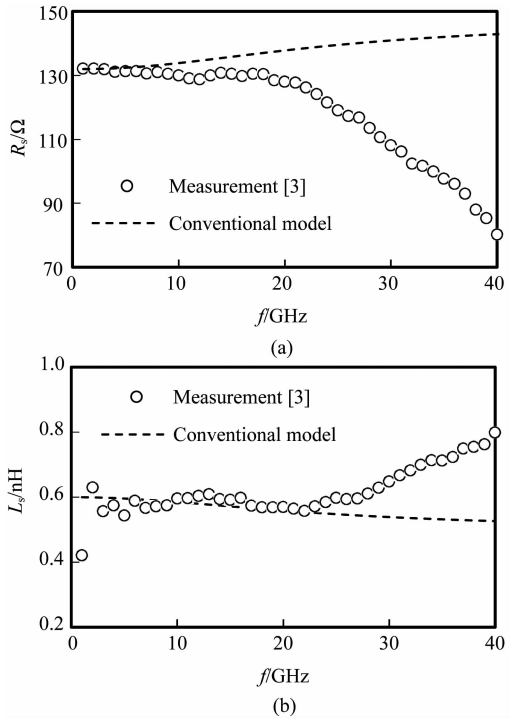

Fig. 4　Comparison of (a) equivalent series resistance, and (b) series inductance between the measurement and conventional model
图 4　测试结果和传统模型关于(a)等效串联电阻，(b)等效串联电感的对比图

the rise of series inductance at high frequency, a capacitance C is added in parallel with R_{s0} to model the high-frequency characteristics.

Figure 5 shows the improved equivalent circuit model. For simplifying the following parameter extraction procedure, parasitic effects between graphene and substrate will be neglected. The simplification procedures, referring the transmission matrix that converted from de-embedded S-parameters in Ref. 3, prove that the tested inductor can be reasonably equivalent to the series impedance topology. The equivalent series resistance and inductance in Eq. 1 is analyzed to find out the effect of the parallel capacitance C, they can be expressed as followed:

$$R_s(\omega) = \frac{R_{s0}}{1+\omega^2 C^2 R_{s0}^2} + \frac{\omega^2 R_{s1} L_{s1}^2}{R_{s1}^2+\omega^2 L_{s1}^2}, \quad (5)$$

$$L_s(\omega) = L_{so} - \frac{CR_{s0}^2}{1+\omega^2 C^2 R_{s0}^2} + \frac{R_{s1}^2 L_{s1}}{R_{s1}^2+\omega^2 L_{s1}^2}. \quad (6)$$

Equations 5-6 and the curve of $R_s(f)$ versus frequency with different C value, shown in Fig. 6, provide a qualitative description of the effect of C. Comparing Fig. 4 and Fig. 6, the model without C could not predict the decline of the equivalent series resistance and the rise of equivalent series inductance at high frequency, but the new model with a RC network could. Moreover, the higher value of C intensifies the drop of $R_s(f)$ and the rise of $L_s(f)$. The effect of parallel capacitance C will be quantitatively evaluated in Sect. 2, along with parameter extraction procedures.

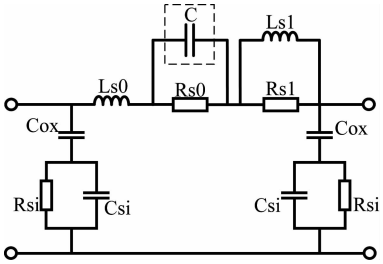

Fig. 5　Improved equivalent circuit model of the graphene inductor
图 5　改进的石墨烯电感等效电路模型

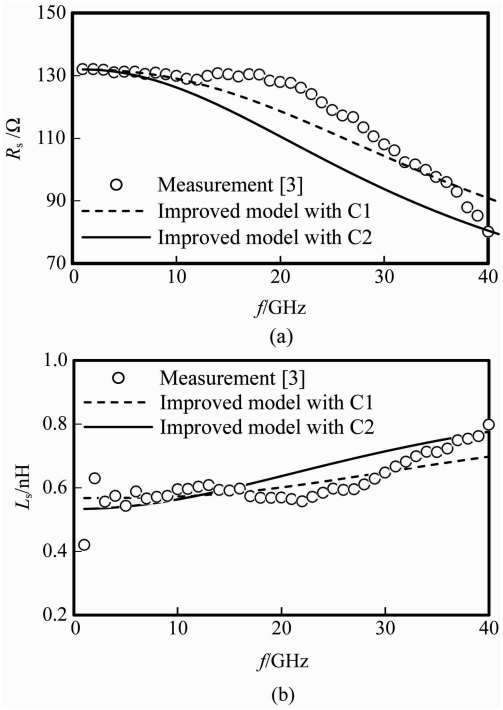

Fig. 6　Comparison of (a) equivalent series resistance, and (b) series inductance between the measurement and improved model ($C2$ is larger than $C1$)
图 6　测试结果和改进模型关于(a)等效串联电阻和(b)等效串联电感的对比图($C2$ 大于 $C1$)

2　Parameter extraction

Firstly, from Fig. 5, the equivalent series resistance and inductance can be expressed as Eqs. 5-6. The DC resistance and inductance are then equal to Eqs. 5-6 evaluated at $\omega = 0$

$$R_{dc} = R_{s0}, \quad (7)$$

$$L_{dc} = L_{s0} + L_{s1} - CR_{s0}^2. \quad (8)$$

From Eqs. 5-6, R_{s0} and L_{s0} in Eqs. 7-8 can be replaced by the measured R_{dc} and L_{dc}, so we have

$$R_s(\omega) = \frac{\omega^2 R_{s1} L_{s1}^2}{R_{s1}^2+\omega^2 L_{s1}^2} + \frac{R_{dc}}{1+\omega^2 C^2 R_{dc}^2}, \quad (9)$$

$$L_s(\omega) = L_{dc} - \frac{\omega^2 L_{s1}^3}{R_{s1}^2+\omega^2 L_{s1}^2} + \frac{\omega^2 C^3 R_{dc}^4}{1+\omega^2 C^2 R_{dc}^2}. \quad (10)$$

The range of R_{s1} can be obtained from Eqs. 3-4 in the conventional circuit model. After neglecting the small high-order ω^2-terms, we have:

$$R_{s1} = \frac{1}{10} R_{dc} \left(\frac{\omega}{\omega_{crit}}\right)^2 \quad . \quad (11)$$

For a certain C value, two frequency points, near the center point of $R_s(f)$ rising range, are needed to extract R_{s1} and L_{s1}.

At frequency f_1, we have:

$$R_s(\omega_1) = \frac{\omega_1^2 R_{s1} L_{s1}^2}{R_{s1}^2 + \omega_1^2 L_{s1}^2} + \frac{R_{dc}}{1 + \omega_1^2 C^2 R_{dc}^2} \quad . \quad (12)$$

At frequency f_2:

$$L_s(\omega_2) = L_{dc} - \frac{\omega_2^2 L_{s1}^3}{R_{s1}^2 + \omega_2^2 L_{s1}^2} + \frac{\omega_2^2 C^3 R_{dc}^4}{1 + \omega_2^2 C^2 R_{dc}^2} \quad . \quad (13)$$

By solving Eqs. 12-13, R_{s1} and L_{s1} can be determined. The value of R_{s0} and L_{s0} can then be calculated from Eqs. 7-8.

The extracting process is illustrated as Fig. 7. Firstly, R_{dc} and L_{dc} are measured at low frequencies, and the range of R_{s1} is determined. Then set the initial value of C, the value of R_{s0}, L_{s0}, R_{s1} and L_{s1} obtained using Eqs. 7-8, 12-13. The value of C is updated to reduce the errors of the simulated and the measured S-parameters.

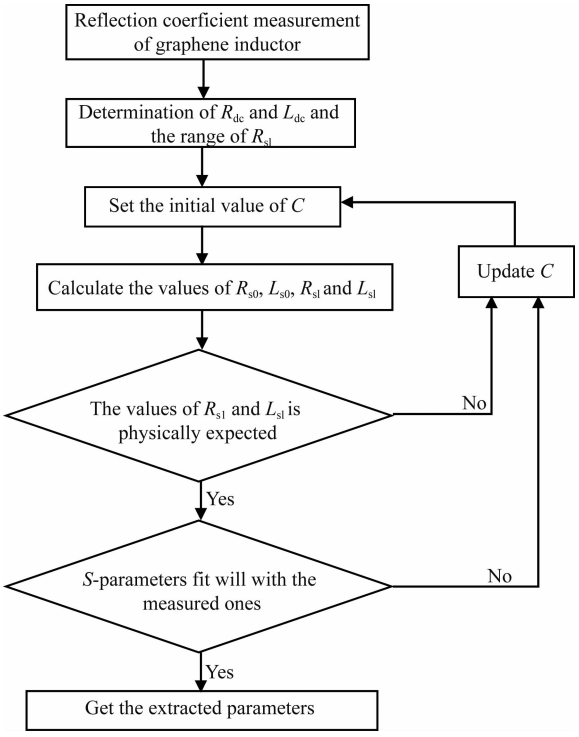

Fig. 7 The flow chart of extracting parameters
图7 参数提取流程图

3 Results and discussion

To verify the modeling and parameter extraction methodology proposed in this paper, we apply it to extract parameters of an 3/4-turn graphene inductor with the outer diameter being 24 μm, the trace width 3 μm and the turn pitch 62 nm. The S-parameters were measured with a commercial ground-signal-ground (GSG)[15], using Agilent N 5 227 A Network Analyzer and a microwave probe station equipped with Cascade Infinity GSG-probes[3]. Advanced Design System (ADS) is then used to simulate the equivalent circuit model. An agreement is performed to S_{11} in order to extract the fitted circuit parameters for a given device.

Figure 8 shows the elements R_{s1}, L_{s0} and L_{s1} versus C. It can be found that R_{s1} and L_{s1} increase with the increase of C. The magnitude variation of L_{s0} is very small. From Eq. 7, R_{s0} is constant and equal to R_{dc}. From Eq. 11, we can obtain that the maximum value of R_{s1} is 47.5 Ω. Therefore, the corresponding C is the range of 21.2 ~ 35.7 fF.

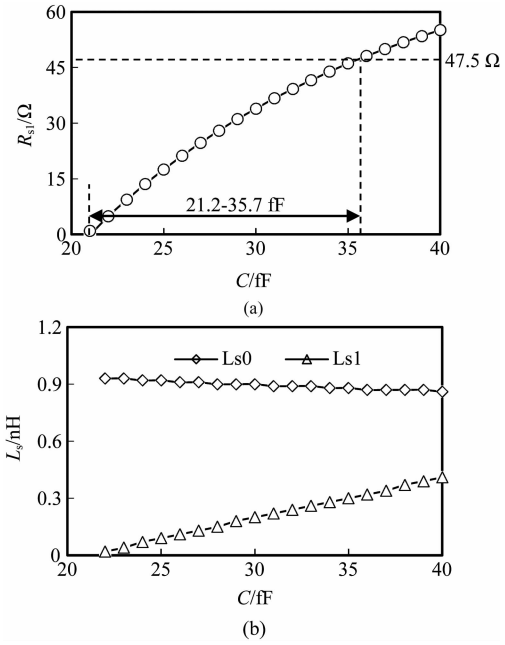

Fig. 8 Extracted parameters R_{s1}, L_{s0} and L_{s1} versus C
图8 参数 R_{s1}, L_{s0} 和随 C 变化曲线图

To represent the fitness between measured and modeled S-parameters, the error functions are defined as

$$\Delta S_{pq}^N = |S_{pq}^N - S_{pq}^M| / |S_{pq}^M| \quad , \quad (14)$$

$$\Delta S_{pq}^C = |S_{pq}^C - S_{pq}^M| / |S_{pq}^M| \quad . \quad (15)$$

S_{pq}^M represents the measured S-parameters. S_{pq}^N represents the S-parameters of new equivalent circuit model. S_{pq}^C represents the S-parameters of conventional model.

Figure 9 shows the mean errors and maximum errors of S_{11} and S_{12} versus C between 20 ~ 40 GHz. It can be observed that, in the range of 21.2 ~ 35.7 fF, the lowest mean error is obtained at 30 fF while the lowest maximum error at 33 fF. And the optimum value of C is 30 fF for all concerned. The value of the fitted parameters for the graphene inductor are shown in Table 1.

Figure 10 shows the comparison of modeled and measured S-parameters and Q values up to 40 GHz. Good agreements are obtained over the whole frequency range, it demonstrate the accuracy of the extracted values.

Table 1　Extraction elements of graphene inductor
表 1　石墨烯电感所提取的参数

Elements	C/fF	R_{s0}/Ω	R_{s1}/Ω	L_{s0}/nH	L_{s1}/nH
Values	30	132	33.9	0.9	0.2

Figure 11 shows the comparison of S_{11} and S_{12} error percentage between the two models. It can be observed that the proposed model can describe the characteristics of graphene inductor more accurately than the conventional one. The error percentage of conventional model rises dramatically, while the S_{11} and S_{12} error of proposed model are below 6% and 13% in the frequency range, respectively.

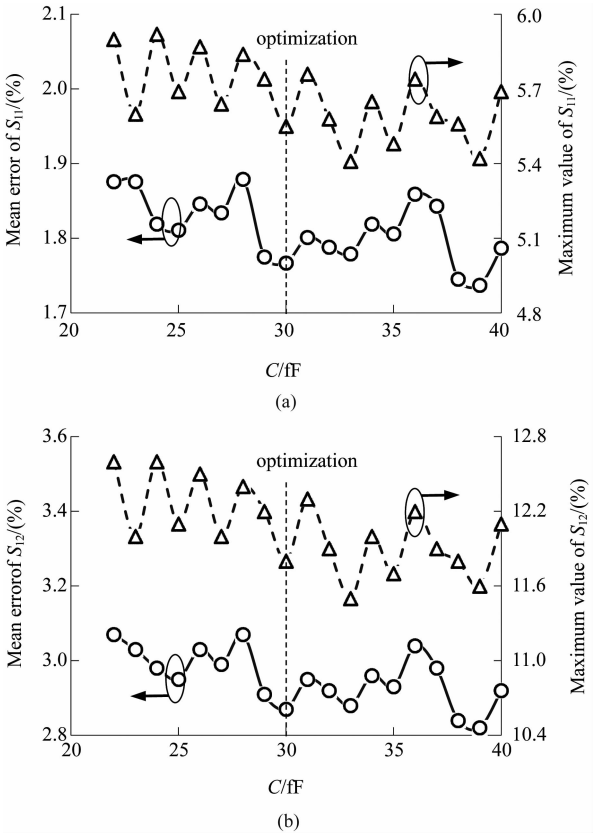

Fig. 9　(a) S_{11} errors and (b) S_{12} errors versus C
图 9　S_{11} 和 S_{12} 参数误差值随 C 变化曲线图

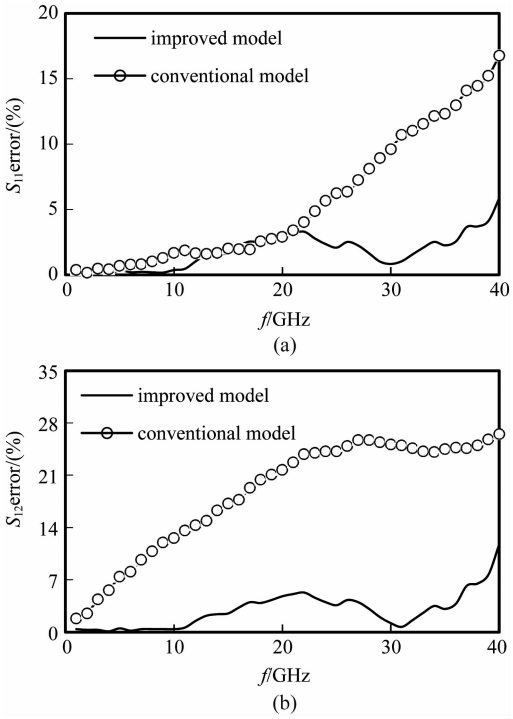

Fig. 11　Comparison of S-parameters errors between conventional (Fig. 3) and improved (Fig. 5) equivalent circuit model
图 11　传统模型(图 3)和改进模型(图 5)的 S 参数误差对比图

4　Conclusion

In this paper, we have proposed an improved equivalent circuit model for graphene on-chip inductors based on physical structure. A parameter extraction method for the simplified model is developed. The validity of the new approach is proven by comparison between measured and simulated S-parameter in the frequency range of 1 ~ 40 GHz.

Acknowledgements

This work was supported in part by National Natural Science Foundation of China under Grant No. 61474044.

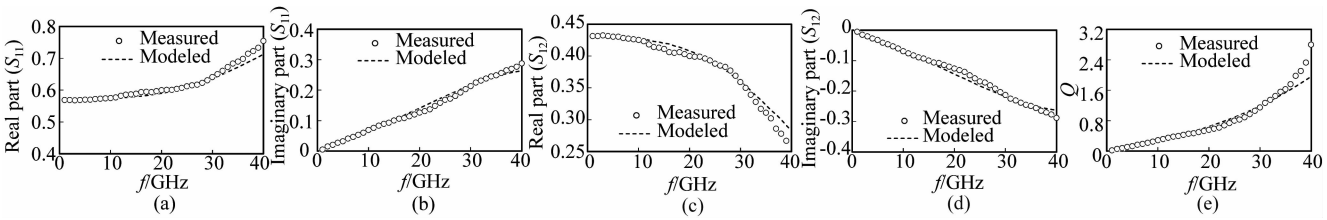

Fig. 10　Comparison of modeled and measured S-parameters and Q value
图 10　模型仿真和测试结果的 S 参数和 Q 值对比图

References

[1] Burghartz J, Edelstein D, Soyuer M, *et al*. RF circuit design aspects of spiral inductors on silicon [J]. *IEEE J. Solid-State Circuits*, 1998, **33**(12):2028 - 2034.

[2] Gil J, Shin H. A simple wide-band on-chip inductor model for silicon-based RF ICs [J]. *IEEE Trans. Microwave Theory Tech.*, 2003, **51**(9):2023 - 2028.

[3] Li X, Kang J, Xie X, *et al*. Graphene inductors for high-frequency applications-design, fabrication, characterization, and study of skin effect [C]. *IEDM Thch. Dig.*, 2014:5.4.1 - 5.4.4.

[4] Sarkar D, Xu C, Li H, *et al*. High-frequency behavior of grapheme based interconnects-Part I: Impedance modeling [J]. *IEEE Trans. Electron Devices*, 2011, **58**(3):843 - 852.

[5] Sarkar D, *et al*. High-frequency behavior of grapheme based interconnects-Part II: Impedance analysis and implications for inductor design [J]. *IEEE Trans. Electron Devices*, 2011, **58**(3):583 - 859.

[6] Gao J, Yang C. Microwave modeling and parameter extraction method for multilayer on-chip inductors [J]. *International Journal of RF and Microwave Computer-Aided Engineering*, 2013, **23**(3):343 - 348.

[7] Yue C P, Wong S S. Physical modeling of spiral inductors on silicon [J]. *IEEE Tran. Electron Devices*, 2000, **47**(3):560 - 568.

[8] Guo J C, Tan T Y. A broadband and scalable model for on-chip inductors incorporating substrate and conductor loss effects [J]. *IEEE Tran. Electron Device*, 2006, **53**(3):413 - 421.

[9] Yang G, Wang Z, Wang K. Modified T-model with an improved parameter extraction method for silicon-based spiral inductors [J]. *IEEE Microwave and Wireless Components Letters*, 2014, **24**(11):817 - 819.

[10] Cao Y, Groves R A, Huang X, *et al*. Frequency-independent equivalent-circuit model for on-chip spiral inductors [J]. *IEEE J. Solid-State Circuits*, 2003, **38**(3):419 - 426.

[11] Huang F, Lu J, Jiang D, *et al*. A novel analytical approach to parameter extraction for on-chip spiral inductors taking into account high- order parasitic effect [J]. *Solid-State Electronics*, 2006, **50**:1557 - 1562.

[12] Chen H, Zhang H, Chung S, *et al*. Accurate systematic model-parameter extraction for on-chip spiral inductors [J]. *IEEE Trans. Electron Devices*, 2008, **55**(11):3267 - 3273.

[13] Kuhn W B, Ibrahim N M. Analysis of current crowding effects in multiturn spiral inductors [J]. *IEEE Trans. Microwave Theory Tech.*, 2001, **49**(1):31 - 38.

[14] Kang M, Gil J, Shin H. A simple parameter extraction method of spiral on-chip inductors [J]. *IEEE Tran. Electron Devices*, 2005, **52**(9):1976 - 1981.

[15] ZHOU Ying, YU Pan-Pan, GAO Jian-Jun. Radio-frequency modeling and parameters extraction of multi-cell MOSFET device [J]. *J. Infrared Millim. Waves* (周影,于盼盼,高建军. 多胞 MOSFET 器件的射频建模和参数提取. **红外与毫米波学报**), 2017, **36**(5):550 - 553.